Ceramics International xxx (xxxx) xxx

Contents lists available at ScienceDirect

Ceramics International

journal homepage: www.elsevier.com/locate/ceramint

Short communication

Crystal structure, infrared spectra, and microwave dielectric properties of the $EuNbO_4$ ceramic

Lintao Liu [a], Yueguang Chen [b], Zhanbai Feng [c], Haitao Wu [a,*], Xiaoyu Zhang [a,**]

[a] School of Environment and Material Engineering, Yantai University, Yantai, 264005, Shandong, China
[b] Shandong Tongfang Luying Electronic Co., Ltd., Yinan, 276300, Shandong, China
[c] School of Materials Science and Engineering, University of Jinan, Jinan, 250022, China

ARTICLE INFO

Keywords:
EuNbO4
Infrared spectra
Microwave dielectric properties
Chemical bond theory

ABSTRACT

The novel microwave dielectric ceramic $EuNbO_4$ with monoclinic structure (PDF # 22-1099) was synthesized using the conventional solid-state reaction process. X-ray diffraction and Rietveld refinement were employed to investigate the phase compositions and crystal parameters. Combined with the refinement results, the structure-property relationship was analyzed using the chemical bonds theory of complex crystals. The surface micro-topography was characterized using scanning electric microscope, and the dense and homogeneous micro-structures could be observed at $EuNbO_4$ ceramic sintered at 1125 °C. Infrared reflectivity spectra indicated the absorption of structural phonon oscillation might be the main contribution to polarization for EuNbO4 ceramic. The optimal dielectric properties with $\varepsilon_r = 19.1$, $Q \times f = 15{,}014$ GHz, and $\tau_f = -16.42$ ppm/°C were achieved in $EuNbO_4$ ceramic sintered at 1125 °C.

1. Introduction

Microwave dielectric ceramics are widely used in GPS antenna technology, dielectric waveguide circuit, radar, and wireless communication devices. Recently, the continuous development of 5G telecommunications technology have put forward higher demands for microwave dielectric materials [1,2]. Microwave dielectric materials are required to have a proper dielectric constant for the miniaturization of devices, a high-quality factor to meet the frequency selective bandwidth and a near-zero temperature coefficient of resonant frequency for environmental stability [2–5]. Researchers have made great efforts to achieve excellent microwave dielectric materials, including the finding of new material systems, improvements on properties by ion substitution and the enhancements on sintering characteristics by adding sintering additives [6–14]. However, there is still a need to search for new materials with high performance for wireless communication application [15–17]. Furthermore, the relationships between dielectric properties and structures also need to be investigated.

Recently rare-earth orthoniobates (RENbO4) have attracted much attention because of their mixed protonic, native ionic, and electronic conduction properties. Siqueira et al. studied the crystal structure of lanthanide orthoniobates by vibrational spectroscopy and determined the Raman active modes [18]. The microwave dielectric properties of a series of $RENbO_4$ ceramics have been reported [19,20]. For example, $(Nd_{0.9}Bi_{0.1})NbO_4$ ceramic exhibited a well microwave dielectric properties of $\varepsilon_r = 22.5$, $Q \times f = 50{,}000$ GHz and $\tau_f = -9$ ppm/°C was obtained at 1150 °C [19]. $LaNbO_4$ ceramics with the dielectric properties of $\varepsilon_r = 20.26$, $Q \times f = 59{,}740$ GHz, and a positive value of $\tau_f = 7.44$ ppm/°C were obtained at 1275 °C [20]. The $RENbO_4$ ceramics presented excellent dielectric properties, indicating grate potential at the application of microwave communication devices. Therefore, it is necessary to develop new $RENbO_4$ microwave dielectric ceramics.

According to Chen's report, $EuNbO_4$ is a promising high-temperature thermal barrier coating [21]. It also possesses excellent photoluminescence properties. However, to the best of our knowledge, there are no reports on the microwave dielectric properties of $EuNbO_4$ ceramic. In this work, the $EuNbO_4$ (ENO) materials were successfully fabricated via the classic solid-state reaction process. The sintering behaviors and the structural features of ENO ceramics were analyzed using XRD, SEM, and Rietveld refinement systematically. Based on the crystal parameters and the complex crystals chemical bonds theory, the intrinsic factors (i.e., bond energy) were calculated, and infrared (IR)

* Corresponding author.
** Corresponding author.
E-mail addresses: mse_wuht@ujn.edu.cn (H. Wu), zhangxiaoyu@ytu.edu.cn (X. Zhang).

https://doi.org/10.1016/j.ceramint.2020.09.176
Received 21 July 2020; Received in revised form 23 August 2020; Accepted 18 September 2020
Available online 21 September 2020

reflectivity spectra were used to investigate the effects of vibration modes on the dielectric properties of ENO ceramics.

2. Experimental procedure

The raw powders of Eu_2O_3 (99.9%, Aladdin) and Nb_2O_5 (99.9%, Aladdin) were stoichiometrically weighed and placed into a nylon jar and ground using some ZrO_2 balls in alcohol for 24 h. After drying, the well-mixed raw materials were calcined at 1100 °C and subjected to ball grinding again. Paraffin (8 wt%) was added as adhesive into the granulated powders and pressed to cylindrical samples with the diameter and height of 10 and about 5 mm, respectively. These pellets were calcined at 500 °C for 4 h and sintered at different temperatures (1050 °C-1150 °C) in the air to remove the adhesive.

The phase compositions and microstructures of ENO materials were carried out using an X-ray diffractometer (XRD: Brucker D8, GER) and a field-emission scanning electron microscope (SEM; Quanta 250, FEI Co., USA), respectively. Fourier transform IR spectroscopy (Bruker IFS 66v, GER) was used to collect the signals of the IR reflectivity spectra of the ENO samples. The dielectric constants (ε_r) and quality factors ($Q \times f$) were tested via the network analyzer (N5234A, Agilent Co., USA) to characterize the microwave dielectric properties of ENO materials [22, 23]. The temperature coefficient of the resonant frequency (τ_f) was calculated using Eq. (1):

$$\tau_f = \frac{f_{85} - f_{25}}{f25 \times 60} \times 10^6 \left(ppm \Big/ {}^{\circ}C \right) \quad (1)$$

f_{25} and f_{85} are the resonant frequencies at the operating temperatures of 25 °C and 85 °C, respectively. The apparent density was used to characterize the sintering behaviors of the ENO specimens and obtained via the Archimedes method (XS64, Mettler Toledo, USA).

3. Results and discussion

The XRD patterns of the ENO specimens obtained at 1050 °C–1150 °C are shown in Fig. 1(a). All diffraction peak positions were matched well with the standard diffraction card (PDF # 22-1099). The ENO specimens were identified to the monoclinic structure with the space group $C2/c$, and no secondary phase was observed. These results indicated that the These results indicated that single $EuNbO_4$ phase was formed successfully. The XRD patterns of the ENO specimen sintered at 1125 °C were refined by the Rietveld refinement to further study the crystalline structure. The results are shown in Fig. 1(b). Rietveld refinements were carried out by *FullProf* software, and the structure parameters were obtained with $a = 5.3927$ Å, $b = 11.1263$ Å, $c = 5.1122$ Å, $\alpha = \gamma = 90.0000°$, $\beta = 94.6470°$, and $V_m = 305.7237$ Å^3. The schematic of the ENO cell structure is shown in Fig. 1(c). Eu^{3+} and Nb^{5+} were surrounded by O^{2-} constituting EuO_8-dodecahedron and NbO_4- tetrahedron, and the dodecahedrons were connected with the tetrahedrons via edge.

Fig. 2(a–e) shows the surface morphology of the experimentally obtained ENO ceramics. The results have shown that the ENO ceramic with clear grain boundary was achieved. With the sintering temperature increasing, the average grain size of the ENO ceramic increased slightly. The pore's variations were attributed to the increasing sintering temperature and gradually vanished, which was different from specimen to specimen. And the decreased of pores is responsible for the increasing of the grain size. The homogeneous grains without pores were obtained at 1125 °C. As the sintering temperature further increased, the grain boundaries were blurred, which might cause negative effects on the dielectric properties.

The temperature-dependent diametric shrinkage ratio and the apparent density of the ENO specimens are plotted in Fig. 3(a). With increasing sintering temperature, the apparent density of ENO specimens initially reached maximum values (6.295 g cm^{-3}) at 1100 °C and finally decreased slightly in 1125 °C–1150 °C. Along with pores gradually eliminated, the diametric shrinkage ratio increased, and have reached the maximum value of 13.77% at 1125 °C. As a result, the extrinsic factors could be ignored and the intrinsic factors would have a great influence on the dielectric properties for the samples sintered at 1125 °C.

Fig. 3(b) shows the dependence among ε_r, $Q \times f$, and τ_f with varying sintering temperature. From the curves of the dielectric properties of the ENO ceramics, the optimum performance can be obtained at 1125 °C. With sintering temperature increased from 1050 °C to 1125 °C, the ε_r of the ENO ceramics gradually increased from 18.27 to 19.1 and then decreased at 1150 °C. The maximum ε_r of 19.1 was obtained at 1125 °C. The permittivity of air is about 1, which is much smaller than that of ceramics. The increase in ε_r can be explained by the decreased of pores, and the decrease in ε_r was attributed to the blurred grain boundaries at

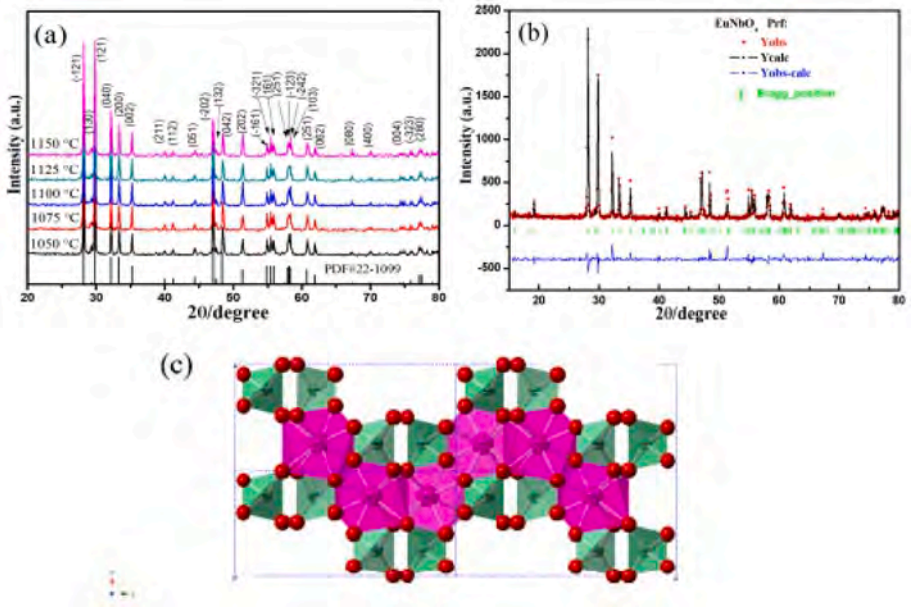

Fig. 1. (a) The X-ray diffraction patterns of the $EuNbO_4$ ceramic sintered at 1050 °C–1150 °C for 4 h. (b) The Rietveld refinement of the $EuNbO_4$ ceramic sintered at 1125 °C. (c) The schematic of the crystal structure of the $EuNbO_4$ ceramic.

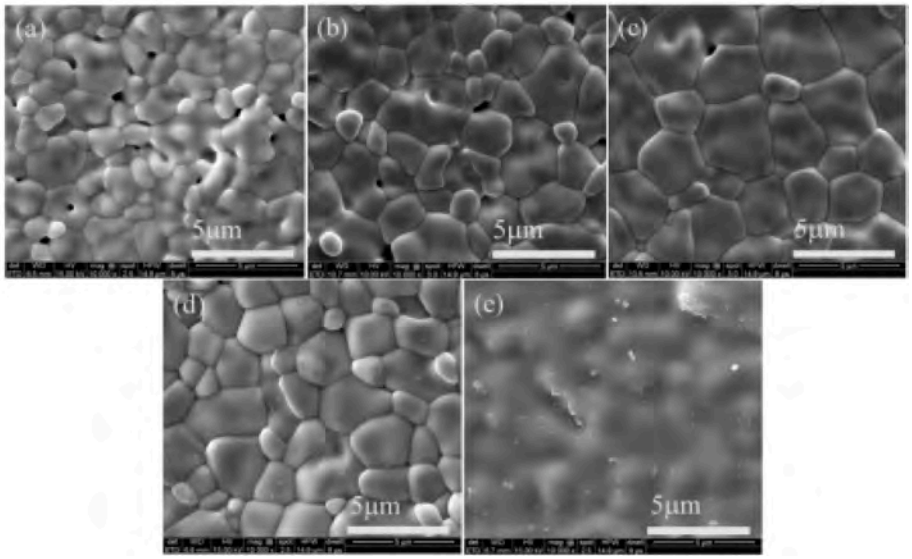

Fig. 2. The SEM micrographs of the $EuNbO_4$ ceramics sintered at 1050 °C–1150 °C for 4 h.

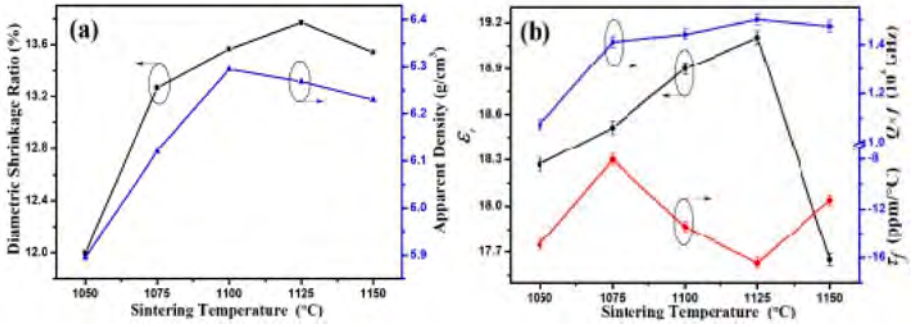

Fig. 3. (a) The apparent densities and diametric shrinkage ratio of $EuNbO_4$ ceramics as a function of sintering temperatures from 1050 °C to 1150 °C. (b) The curves of ε_r, $Q \times f$, and τ_f values for $EuNbO_4$ ceramics sintered at different temperatures.

1150 °C.

As the specimen possessed a high shrinkage ratio, intrinsic factors, such as polarizability, played a major role in affecting the ε_r values. The Clausius–Mossotti equation and the additive rules were used to calculate the polarizability of the compact ENO ceramic (Eqs. [2,3]) [24,25]. The theoretical ($\alpha_{theo.}$) and the observed ($\alpha_{obs.}$) polarizability values were 16.54 and 15.65, respectively. The $\alpha_{theo.}$ was calculated in ideal crystalline. Thus, the minor deviation was inevitable among the results.

$$\alpha_{theo} = \alpha\left(Eu^{3+}\right) + \alpha\left(Nb^{5+}\right) + 4\alpha\left(O^{2-}\right)\alpha_{theo} \tag{2}$$

$$\alpha_{obs} = \frac{1}{b} V_m \frac{\varepsilon_{mea} - 1}{\varepsilon_{mea} + 2} \tag{3}$$

α (Eu^{2+}), α (Nb^{5+}), and α (O^{2-}) are the polarizability values, which refer to the works of Shannon [24]. Moreover, b and V_m indicate $4\pi/3$ and unit cell volume, respectively.

The microwave dielectric properties were influenced by the extrinsic (e.g., density, pores, secondary phase, and impurity) and the intrinsic (e.g., crystalline structure, lattice vibration modes, and lattice defect) factors. The $Q \times f$ of the ENO ceramics under varying sintering temperatures are shown in Fig. 3(b). With increasing temperature from 1050 °C to 1150 °C, the $Q \times f$ value gradually increased from 10,711 GHz to 25,013 GHz and slightly decreased. The variations in the $Q \times f$ value could be explained by the extrinsic losses (pores). In summary, the compact specimens at 1125 °C showed the highest ε_r and highest $Q \times f$. Fig. 3(b) also shows that the τ_f of ENO materials at different temperature changes between −8.028 ppm/°C and −16.416 ppm/°C.

The microwave dielectric properties of Nb-based ceramics that were reported in recent years are summarized in Fig. 4 [20,21,26–40]. As shown in Fig. 4(a), the red point at bottom left The microwave dielectric properties of $EuNbO_4$ ceramic was first investigated. EuNbO4 ceramic sintered at 1300 °C exhibit $\varepsilon_r = 19.1$, $Q \times f = 15{,}014$ GHz, and $\tau_f = -16.42$ ppm/°C. By comparison, the $Q \times f$ of ENO ceramics is relatively inferior, but the value of τ_f is near-zero, which is better than most materials in this system, as shown in Fig. 4(b). It means that the ENO ceramics have great potential for exploitation in enhancing properties. So, it is necessary to research the relations between structure and properties. The compact ENO specimens sintered at 1125 °C possessed a condition that the extrinsic factors could be neglected. Thus, the bond ionicity, bond energy, lattice energy, and thermal expansion coefficients the bonds contained in the ENO crystalline was calculated on the basis of the refinement results, the complex chemical bond theory, and electronegativity. The calculated details were referred to Sanderson's work [41–43].

Based on the complex chemical theory, the complex crystals of ENO could be decomposed into the sum of binary crystals as follows:

$$\begin{aligned} EuNbO_4 &= Eu + Nb + 2O(1) + 2O(2) \\ &= Eu_{1/2}O1) + Eu_{1/2}O2)(2)_{4/3} + Nb_{2/3}O1) + Nb_{1/3}O(2)_{2/3} \end{aligned} \tag{4}$$

The dielectric constant ϵ_r has closely relations with the values of f_i [44]. On the basis of P–V-L theory, the bond ionicity were obtained through Eqs. (5)–(9) [45–47]:

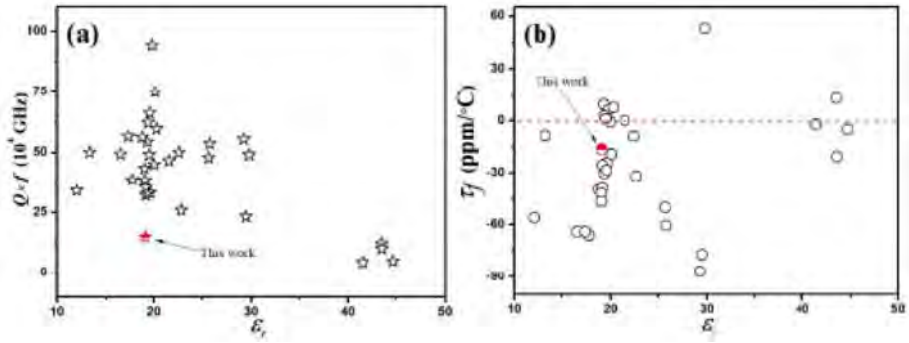

Fig. 4. (a) The $Q \times f$ with e_r of Nb-based ceramics. (b) The τ_f with e_r of Nb-based ceramics.

$$\varepsilon = \frac{n^2 - 1}{1 - f_i} + 1 \tag{5}$$

$$f_i^{\mu} = (C^{\mu})^2 \Big/ \left(E_g^{\mu}\right)^2 \tag{6}$$

$$\left(E_g^{\mu}\right)^2 = \left(E_g^{\mu}\right)^2 + (C^{\mu})^2 \tag{7}$$

$$\left(E_h^{\mu}\right)^2 = \frac{39.74}{(d^{\mu})^{2.48}} \tag{8}$$

$$C^{\mu} = 14.4 b^{\mu} \exp\left(-k_s^{\mu} r_0^{\mu}\right)\left[\left(Z_A^{\mu}\right)^* - \frac{n}{m}\left(Z_B^{\mu}\right)^*\right] \Big/ r_0^{\mu} \tag{9}$$

Where E_{μ}^{g}, E_{μ}^{h} and C^{μ} are the average energy gap, the homopolar part and the heteropolar part, respectively. The part of $exp(-k_s^{\mu} r_0^{\mu})$ is the Thomas-Fermi screening factor [48]. In Table 1, the bond ionicity of *Eu–O* and *Nb–O* were 83.14% and 62.74%, respectively. The bond ionicity was an intrinsic factor in effecting to the dielectric constant. It suggested that the *Eu–O* bond provided a major contribution to the dielectric constant of ENO ceramic.

The bond energy (E) was calculated using Eqs. 10–13. And the calculated results of the ENO ceramics sintered at 1125 °C are shown in Table 1.

$$E = \sum_{\mu} E_b^{\mu} \tag{10}$$

$$E_b^{\mu} = t_c E_c^{\mu} + t_i E_i^{\mu} \tag{11}$$

$$E_c^{\mu} = \frac{(r_{cA} + r_{cB})}{d^{\mu}} \left(E_{A-A} E_{B-B}\right)^{1/2} \tag{12}$$

$$E_i^{\mu} = \frac{33200}{d^{\mu}} \tag{13}$$

The E, as a physical quantity of bond strength, was an intrinsic property of crystal. Based on the calculated results, the E values of the *Eu–O* and the *Nb–O* bonds were 303.727 kJ/mol and 617.327 kJ/mol, respectively. The $E(Eu–O) < E(Nb–O)$ results indicated that the *Nb–O* bonds influenced the $Q \times f$ values.

The lattice energy U of ENO samples could be divided into two parts of U_{bc}^{μ} and U_{bi}^{μ}, and obtained by Eqs. 14–17:

$$U_{cal} = \sum_{\mu} U_b^{\mu} \tag{14}$$

$$U_{\mathrm{b}}^{\mu} = U_{\mathrm{bc}}^{\mu} + U_{\mathrm{bi}}^{\mu} \tag{15}$$

$$U_{\mathrm{bc}}^{\mu} = 2100 m \frac{\left(Z_{+}^{\mu}\right)}{\left(d^{\mu}\right)^{0.75}} \mathrm{f}_c^{\mu} \tag{16}$$

$$U_{bi}^{\mu} = 1270 \frac{(m+n) Z_{+}^{\mu} Z_{-}^{\mu}}{d^{\mu}} \left(1 - \frac{0.4}{d^{\mu}}\right) f_i^{\mu} \tag{17}$$

The intrinsic dielectric loss of crystal resulted in the anharmonic terms of lattice vibration. Lattice energy is defined as the released energy during the process by which gaseous ions combine to form solid state. The ionic bonds with higher the lattice energy are more stable, so the lattice energy stands for the stability of the ionic crystal. The lattice energy as the intrinsic factors take an important role in effecting quality factor values. According to Table 1, the lattice energy of the *Eu–O* and the *Nb–O* bonds were 1409.750 kJ/mol and 10697.500 kJ/mol, respectively. The lattice energy of *Nb–O* bonds is bigger than *Eu–O* bonds, obviously. It indicates that the *Nb–O* bonds take a predominant role in effecting the quality factor of ENO ceramics.

It was well known that the τ_f values are controlled by τ_ε (the temperature coefficient of permittivity) and α (coefficient of thermal expansion). Based on chemical bonds theory of complex crystals, values of thermal expansion coefficient could be calculated by Eq. (18). In practice applications, the near-zero t_f is needed, so the near-zero α was beneficial to the values of t_f. And the value of α is calculated by Eqs. 18–22:

$$\tau_f = -\frac{\tau_\varepsilon}{2} - \alpha \tag{18}$$

Table 1
The bond ionicity (fi), lattice energy (U), bond energy (E) and the coefficient of thermal expansion (α) of each bond for $EuNbO_4$ ceramics sintered at 1125 °C.

Bond Type	d (Å)	f_i (%)	E_i (kJ mol^{-1})	E_c (kJ mol^{-1})	E (kJ mol^{-1})	U (kJ mol^{-1})	α (10^{-6} K^{-1})
Eu1–O1^1 × 2	2.3831	83.08	582.613	145.482	308.678	1421.000	8.440
Eu1–O1^2 × 2	2.4564	83.27	565.227	128.310	291.426	1386.000	8.734
Eu1–O2^1 × 2	2.3659	83.03	586.848	146.540	310.922	1429.000	8.376
Eu1–O2^2 × 2	2.4207	83.18	573.563	143.223	303.883	1403.000	8.589
Nb–O1 × 2	1.9201	62.86	723.100	553.001	605.448	10549.000	0.531
Nb–O2 × 2	1.8476	62.62	751.474	574.701	629.206	10846.000	0.430
Eu–O$^{avg.}$	–	83.14	577.063	140.889	303.727	1409.750	8.535
Nb–O$^{avg.}$	–	62.74	737.287	563.851	617.327	10697.500	0.481

Eu–O$^{avg.}$ is the average of the bond parameters of Eu–O bonds.
Nb–O$^{avg.}$ is the average of the bond parameters of Nb–O bonds.

$$\alpha = \sum_{\mu} F_{mn}^{\mu} \alpha_{mn}^{\mu} \tag{19}$$

$$\alpha_{mn}^{\mu} = -3.1685 + 0.8376\gamma_{mn} \tag{20}$$

$$r_{mn} = \frac{kZ_A^{\mu} N_{CA}^{\mu}}{U_b^{\mu} \Delta_A} \beta_{mn} \tag{21}$$

$$\beta_{mn} = \frac{m(m+n)}{2n} \tag{22}$$

Where F_{MN}^{μ}, N_{CA}^{μ}, Z_A^{μ} and k are the proportion of μ bond, the coordination number of μ bond for cation, the valence states of cation and Boltzmann constant, respectively. The calculated results were shown in Table 1, the a values of the *Eu–O* and the *Nb–O* bonds were 8.535×10^{-6} K^{-1} and 0.481×10^{-6} K^{-1}, respectively. *a(Eu–O) > a(Nb–O)*, indicates that the bond of *Nb–O* was taken predominant contribution to the τ_f of ENO ceramics.

In this work, the intrinsic loss of dielectric properties caused by the lattice vibration phonon modes were studied. The IR reflectivity spectrum was used to study the lattice vibration phonon modes. Fig. 5(a) illustrates the IR reflectivity spectra of the ENO materials sintered at 1125 °C. The complex dielectric function was calculated through the classical oscillator model, and the dielectric loss and the complex reflectivity were calculated using Eqs. 23–26.

$$\varepsilon^*(\omega) = \varepsilon_{\infty} + \sum_{j=1}^{n} \frac{\omega_{pj^2}}{\omega_{oj^2} - \omega^2 - j\gamma_j\omega} \tag{23}$$

$$R(\omega) = \left| \frac{1 - \sqrt{\varepsilon^*(\omega)}}{1 + \sqrt{\varepsilon^*(\omega)}} \right|^2 \tag{24}$$

$$\tan\delta = \frac{\varepsilon'}{\varepsilon''} = \frac{\sum_j \Delta\varepsilon_j'(r_j\omega) \Big/ \omega_j^2}{\varepsilon_{\infty} + \sum_j \varepsilon_j'(\omega)} \tag{25}$$

$$\varepsilon'' = \sum_{j=1}^{n} \frac{s_j r_j}{\omega_j^2} \omega \tag{26}$$

The fitting results and dielectric contributions from the 22 resonant modes are shown Table 2. The vibration modes of the far-IR region (below 400 cm^{-1}) had the highest contribution (82.3688%) in the effects to the complex relative ε_r values. The fitting and the measured values of IR reflectivity spectra matched well. Results are shown in Fig. 5 (a). Furthermore, the real and the imaginary parts of ε_r values were calculated. Results are shown in Fig. 5(b). The calculated real parts of the ε_r values ($\varepsilon' = 13.4367$) were lower than the measured values ($\varepsilon'_{mea.} = 19.1031$), and the calculated imaginary parts of the ε_r values (the dielectric loss, $\varepsilon'' = 1.36 \times 10^{-3}$) was similar to the measured values ($\varepsilon''_{mea.} = 8.01 \times 10^{-3}$). According to the above results, the main source of polarization of the ENO ceramics was the absorption of phonon oscillations.

Table 2
The phonon parameters obtained from the fitting of the infrared spectra of $EuNbO_4$ ceramics.

Modes	$EuNbO_4$ $\varepsilon_{\infty} = 3.181$				
	ω_{oj}	ω_{pj}	γ_j	$\Delta\varepsilon_j$	$\Delta\varepsilon_j/\varepsilon_j$ (%)
1	149.9609	337.5557	49.3021	5.0668	49.4076
2	156.7497	98.9573	7.2496	0.3985	3.8859
3	173.0481	97.5765	10.4506	0.3179	3.0999
4	186.6640	70.1722	11.6551	0.1413	1.3779
5	210.6387	233.6666	27.1429	1.2306	11.9999
6	243.9285	89.5323	12.0007	0.1347	1.3135
7	271.3717	158.5965	48.3899	0.3416	3.3310
8	281.1894	51.2028	17.5244	0.0332	0.3237
9	335.6757	209.0450	26.8641	0.3878	3.7815
10	361.2150	140.3721	28.9499	0.1510	1.4724
11	383.6065	189.3507	29.2177	0.2436	2.3754
12	403.7236	74.9539	12.7548	0.0345	0.3364
13	437.4125	159.3837	32.8452	0.1328	1.2950
14	458.3990	176.2677	30.4213	0.1479	1.4422
15	527.8218	51.9872	9.6570	0.0097	0.0946
16	528.9483	227.3343	46.4806	0.1847	1.8011
17	574.7713	267.4508	35.1940	0.2165	2.1111
18	593.6320	246.2196	33.5238	0.1720	1.6772
19	632.0526	553.0002	53.6028	0.7655	7.4646
20	693.6241	199.7396	77.6855	0.0829	0.8084
21	759.0992	121.7112	59.3761	0.0257	0.2506
22	801.4252	151.9454	34.1966	0.0359	0.3501

4. Conclusions

The ENO dielectric ceramics were fabricated via the conventional solid-state reaction process. A pure phase with monoclinic structure (PDF # 22-1099) with the space group *C2/c* was identified using XRD and Rietveld refinement. The specimen sintered at 1125 °C exhibits homogenous and compact grains, which was analyzed by SEM. The ε_r and the $Q \times f$ values were positively related to the diametric shrinkage ratio of the specimens. In addition, the *Nb–O* bonds played a key role in affecting the dielectric properties. Based on infrared reflective spectrum analysis, the main source of polarization of the specimen was the phonon oscillation absorption. The excellent microwave dielectric properties of with $\varepsilon_r = 19.1$, $Q \times f = 15{,}014$ GHz, and $\tau_f = -16.42$ ppm/°C were obtained in the ENO ceramics sintered at 1125 °C.

Declaration of competing interest

The authors declare that they have no known competing financial interests or personal relationships that could have appeared to influence the work reported in this paper.

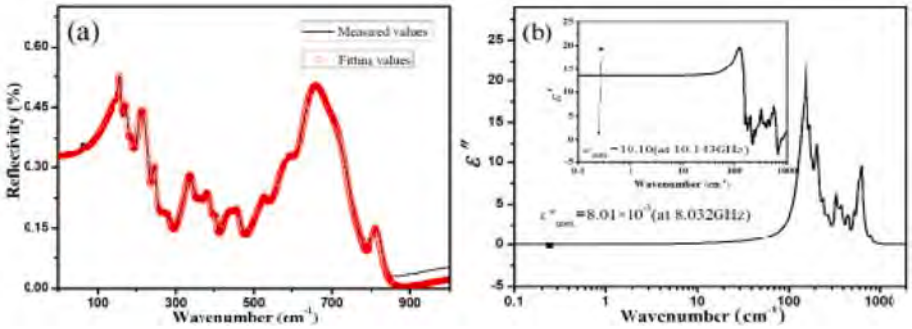

Fig. 5. (a) The measured and fitted infrared reflectivity spectra of $EuNbO_4$ ceramics sintered at 1125 °C. (b) The real and imaginary parts of complex permittivity for $EuNbO_4$ ceramics sintered at 1125 °C.

Acknowledgement

This work was supported by the National Natural Science Foundation (No. 51972143). The authors are also thankful to Professor Zeming Qi and Chuansheng Hu in IR beamline workstation of National Synchrotron Radiation Laboratory (NSRL) for the IR measurement.

References

[1] D. Zhou, L.X. Pang, D.W. Wang, C. Li, B.B. Jin, I.M. Reaney, High permittivity and low loss microwave dielectrics suitable for 5G resonators and low temperature co-fired ceramic architecture, J. Mater. Chem. C 5 (2017) 10094–10098.
[2] H. Ohsato, Functional advances of microwave dielectrics for next generation, Ceram. Int. 38 (2012) S141–S146.
[3] J.X. Bi, C.F. Xing, C.H. Yang, H.T. Wu, Phase composition, microstructure and microwave dielectric properties of rock salt structured Li_2ZrO_3-MgO ceramics, J. Eur. Ceram. Soc. 38 (2018) 3840–3846.
[4] J.J. Zheng, Y.K. Yang, H.T. Wu, Y.Y. Zhou, Z.L. Zhang, Structure, infrared spectra and microwave dielectric properties of the novel Eu_2TiO_5 ceramics, J. Am. Ceram. Soc. 103 (2020) 4333–4341.
[5] J. Li, L. Fang, H. Luo, J. Khaliq, Y. Tang, C.C. Li, Li_4WO_5: a temperature stable low-firing microwave dielectric ceramic with rock salt structure, J. Eur. Ceram. Soc. 36 (2016) 243–246.
[6] T.Y. Qin, C.W. Zhong, Y. Qin, B. Tang, S.R. Zhang, Low-temperature sintering mechanism and microwave dielectric properties of $ZnAl_2O_4$-LMZBS composites, J. Alloys Compd. 797 (2019) 744–753.
[7] H.I. Hsiang, C.C. Chen, S.Y. Yang, Microwave dielectric properties of $Ca_{0.7}Nd_{0.2}TiO_3$ ceramic-filled CaO-B_2O_3-SiO_2 glass for LTCC applications, J. Adv. Ceram. 8 (2019) 345–351.
[8] L. Fang, C.X. Su, H.F. Zhou, Z.H. Wei, H. Zhang, Novel low-firing microwave dielectric ceramic $LiCa_3MgV_3O_{12}$ with low dielectric loss, J. Am. Ceram. Soc. 96 (2013) 688–690.
[9] X.L. Chen, X. Li, H.F. Zhou, J. Sun, X.X. Li, X. Yan, C.C. Sun, J.P. Shi, Phase evolution, microstructure, electric properties of $(Ba_{1-x}Bi_{0.67x}Na_{0.33x})(Ti_{1-x}Bi_{0.33x}Sn_{0.67x})O_3$ ceramics, J. Adv. Ceram. 8 (2019) 427–437.
[10] F.Y. Huang, H. Su, Y.X. Li, H.W. Zhang, X.L. Tang, Low-temperature sintering and microwave dielectric properties of $CaMg_{1-x}Li_{2x}Si_2O_6$ (x=0-0.3) ceramics, J. Adv. Ceram. 9 (2020) 471–480.
[11] H.H. Guo, D. Zhou, W.F. Liu, L.X. Pang, D.W. Wang, J.Z. Su, Z.M. Qi, Microwave dielectric properties of temperature-stable zircon-type (Bi, Ce)VO_4 solid solution ceramics, J. Am. Ceram. Soc. 103 (2020) 423–431.
[12] L. Fang, Z.H. Wei, C.X. Su, F. Xiang, H. Zhang, Novel low-firing microwave dielectric ceramics: $BaMV_2O_7$ (M = Mg, Zn), Ceram. Int. 40 (2014) 16835–16839.
[13] M.J. Wu, Y.C. Zhang, M.Q. Xiang, Synthesis, characterization and dielectric properties of a novel temperature stable $(1-x)CoTiNb_2O_8-xZnNb_2O_6$ ceramic, J. Adv. Ceram. 8 (2019) 228–237.
[14] H.H. Guo, D. Zhou, L.X. Pang, Z.M. Qi, Microwave dielectric properties of low firing temperature stable scheelite structured (Ca,Bi)(Mo,V)O_4 solid solution ceramics for LTCC applications, J. Eur. Ceram. Soc. 39 (2019) 2365–2373.
[15] Y.H. Zhang, H.T. Wu, Crystal structure and microwave dielectric properties of $La_2(Zr_{1-x}Ti_x)_3(MoO_4)_9$ ($0 \le x \le 0.1$) ceramics, J. Am. Ceram. Soc. 102 (2019) 4092–4102.
[16] Y.H. Zhang, J.J. Sun, N. Dai, Z.C. Wu, H.T. Wu, C.H. Yang, Crystal structure, infrared spectra and microwave dielectric properties of novel extra low-temperature fired $Eu_2Zr_3(MoO_4)_9$ ceramics, J. Eur. Ceram. Soc. 39 (2019) 1127–1131.
[17] H.C. Xiang, C.C. Li, H. Jantunen, L. Fang, A.E. Hill, Ultralow loss $CaMgGeO_4$ microwave dielectric ceramic and its chemical compatibility with silver electrodes for low-temperature cofired ceramic applications, ACS Sustain. Chem. Eng. 6 (2018) 6458–6466.
[18] K.P.F. Siqueira, Roberto L. Moreira, Dias Anderson, Synthesis and crystal structure of lanthanide orthoniobates studied by vibrational spectroscopy, Chem. Mater. 22 (2010) 2668–2674.
[19] L.X. Pang, D. Zhou, Modification of $NdNbO_4$ microwave dielectric ceramic by Bi substitutions, J. Am. Ceram. Soc. 102 (2019) 2278–2282.
[20] M. Xiao, P. Zhang, J. Lou, Y.S. Wei, P. Zhang, Combined synthesis methods for producing $LaNbO_4$ ceramics and investigation of microwave dielectric properties based on complex chemical bond theory, J. Alloys Compd. 812 (2020) 152154.
[21] L. Chen, J. Feng, Thermal and mechanical properties optimization of ABO_4 type $EuNbO_4$ by the B-Site substitution of Ta, Engineering 6 (2020) 178–185.
[22] B.W. Hakki, P.D. Coleman, A dielectric resonator method of measuring inductive capacities in the millimeter range, IRE T. Microw. Theory 8 (1960) 402–410.
[23] W.E. Courtney, Analysis and eluation of a method of measuring the complex permittivity and permeability microwave insulators, IEEE T. Microw. Theory 18 (1970) 476–485.
[24] R.D. Shannon, G.R. Rossman, Dielectric constants of silicate garnets and the oxide additivity rule, Am. Mineral. 77 (1992) 94–100.
[25] R.D. Shannon, Dielectric polarizabilities of ions in oxides and fluorides, J. Appl. Phys. 73 (1993) 348–366.
[26] D.-W. Kim, D.-K. Kwon, S.H. Yoon, K.S. Hong, Microwave dielectric properties of rare-earth ortho-niobates with ferroelasticity, J. Am. Ceram. Soc. 89 (2006) 3861–3864.
[27] P. Zhang, Z.K. Song, Y. Wang, L.X. Li, Effect of ion substitution for Nd^{3+} based on structural characteristic on the microwave dielectric properties of $NdNbO_4$ ceramic system, J. Am. Ceram. Soc. 97 (2014) 976–981.
[28] N. Wang, M.Y. Zhao, Z.W. Yin, W. Li, Effects of complex substitution of La and Nd for Bi on the microwave dielectric properties of $BiNbO_4$ ceramics, Mater. Res. Bull. 39 (2004) 439–448.
[29] T.L. Tang, W.S. Xia, B. Zhang, Y. Wang, M.X. Li, L.W. Shi, Optimization on quality factor of $LaNbO_4$ microwave dielectric ceramics, J. Mater. Sci. Mater. Electron. 30 (2019) 15293–15298.
[30] P. Zhang, Y. Zhao, Influence of Sm3+ substitutions for Nd3+ on the microwave dielectric properties of (Nd1−xSmx)NbO4 (x = 0.02–0.15) ceramics, J. Alloys Compd. 654 (2016) 240–245.
[31] Q.J. Mei, C.Y. Li, J.D. Guo, L.P. Zhao, H.T. Wu, Improvements in the sintering behavior and microwave dielectric properties of fergusonite-type $NdNbO_4$ ceramics, Ceram. Int. 41 (2015) 907–912.
[32] S.H. Ding, X. Yao, Y. Yang, Dielectric properties of B_2O_3-doped $BiNbO_4$ ceramics, Ceram. Int. 30 (2004) 1195–1198.
[33] C.M. Cheng, S.H. Lo, C.F. Yang, The effect of CuO on the sintering and properties of $BiNbO_4$ microwave ceramics, Ceram. Int. 26 (2000) 113–117.
[34] M. Xiao, Q.Q. Gu, Z.Q. Zhou, P. Zhang, Study of the microwave dielectric properties of $(La_{1-x}Sm_x)NbO_4$ (x=0-0.10) ceramics via bond valence and packing fraction, J. Am. Ceram. Soc. 100 (2017) 3952–3960.
[35] S.H. Ding, X. Yao, Y. Mao, P.L. Liu, Microwave dielectric properties of $(Bi_{1-x}R_x)NbO_4$ ceramics (R=Ce, Nd, Dy, Er), J. Am. Ceram. Soc. 26 (2006) 2003–2005.
[36] H.Y. Yang, S.R. Zhang, Y.P. Li, H.C. Yang, Y. Yuan, T.L. Wen, E.Z. Li, Investigations of dielectric properties of wolframite $A_{0.5}Zr_{0.5}NbO_4$ ceramics by bond theory and far-infrared spectroscopy, Ceram. Int. 46 (2020) 3688–3694.
[37] E.S. Kim, S.H. Kim, Effects of structural characteristics on microwave dielectric properties of $(1-x)CaWO_4$ –$xLaNbO_4$ ceramics, J. Electroceram. 17 (2006) 471–477.
[38] P. Zhang, T. Wang, W.S. Xia, L.X. Li, Microwave dielectric properties of a new ceramic system $NdNbO_4$ with CaF_2 addition, J. Alloys Compd. 535 (2012) 1–4.
[39] P. Zhang, Y.G. Zhao, L.X. Li, The correlations among bond ionicity, lattice energy and microwave dielectric properties of $(Nd_{1-x}La_x)NbO_4$ ceramics, Phys. Chem. Chem. Phys. 17 (2015) 16692–16698.
[40] H.W. Lee, J.H. Park, S. Nahm, D.W. Kim, J.G. Park, Low-temperature sintering of temperature-stable $LaNbO_4$ microwave dielectric ceramics, Mater. Res. Bull. 45 (2010) 21–24.
[41] R.T. Sanderson, Multiple and single bond energies in inorganic molecules, J. Inorg. Nucl. Chem. 30 (1968) 375–393.
[42] R.T. Sanderson, Chemical Bonds and Bond Energy, Academic Press, New York, 1976.
[43] R.T. Sanderson, Electronegativity and bond energy, J. Am. Ceram. Soc. 105 (1983) 2259–2261.
[44] S.S. Batsanov, Dielectric methods of studying the chemical bond and the concept of electronegativity, Russ. Chem. Rev. 51 (1982) 684–697.
[45] D.F. Xue, S.Y. Zhang, Calculation of the nonlinear optical coefficient of the $NdAl_3(BO_3)_4$ crystal, J. Phys. Condens. Matter 8 (1996) 1949–1956.
[46] Z.J. Wu, Q.B. Meng, S.Y. Zhang, Semiempirical study on the valences of Cu and bond covalency in $Y_{1-x}Ca_xBa_2Cu_3O_{6+y}$, Phys. Rev. B 58 (1998) 958–962.
[47] D.V. Berkov, Evaluation of the energy barrier distribution in many-particle systems using the path integral approach, J. Phys. Condens. Matter 10 (1998) L89–L95.
[48] B.F. Levine, Bond susceptibilities and ionicities in complex crystal structures, J. Chem. Phys. 59 (1973) 1463–1486.